Supporting Information

Schauder et al. 10.1073/pnas.1217549110

SI Materials and Methods

The full-length rat GluK2 subunit cDNA sequence (P42260) including the native signal peptide was cloned into the pFastBac1 vector for baculovirus expression in Sf9 insect cells. The construct was RNA-edited at position 536 (I to V) and had two mutations that increased tetramer expression C545V (M1) and C564S (M1–M2 loop). In the LBD four mutations (A47T, A658S, N690S, and F704L), which convert the sequence to that found in GluK1, were introduced to create a high-affinity binding site for the GluK1 selective antagonist LY466195 (1). For fluorescence detection and affinity purification, a thrombin recognition site and linker sequence (GLVPRGSAAAA) was inserted between GluK2 and the coding sequence for the A207K dimerization-suppressed EGFP mutant, with a C-terminal SGLRHis$_8$ affinity tag. Sf9 cells (12 L) were harvested 72 h after infection, collected by low-speed centrifugation, and frozen at −80 °C. Cell pellets were resuspended in ice-cold buffer (18–20 mL/L) containing 150 mM NaCl, 50 mM Tris (pH 8.0), 0.8 μM aprotinin, 2 μg/mL leupeptin, 2 μM pepstatin, and 1 mM PMSF and then disrupted on ice using a QSonica Q700 sonicator (18 × 15 s, power level 7). The lysate was clarified by low-speed centrifugation and membranes collected by ultracentrifugation (Ti45 rotor, 40,000 rpm, 45 min), followed by mechanical homogenization, and solubilization for 1 h in buffer containing 150 mM NaCl, 20 mM Tris (pH 8.0), 50 mM *n*-dodecyl-β-D-maltopyranoside, and 3.3 mM cholesterol hemisuccinate at 4 °C. Insoluble material was removed by centrifugation (Ti45 rotor, 40,000 rpm, 45 mins) and cobalt-charged TALON metal affinity resin (20 mL) was added to the supernatant together with 10 mM imidazole. After binding for 90 min at 4 °C the resin was packed in a column, washed with buffer containing 150 mM NaCl, 20 mM Tris (pH 8.0), 2 mM *n*-dodecyl-β-D-maltopyranoside, 0.3 mM cholesterol hemisuccinate, and 40 mM imidazole until the OD at 280 nm reached a stable low value, and then eluted with an increase to 250 mM imidazole. Peak fractions were digested overnight at 4 °C with thrombin at a 1:100 wt/wt ratio. GluK2 tetramers isolated by gel filtration chromatography (Superose 6 10/300) in a buffer containing 150 mM NaCl, 20 mM Tris (pH 8.0), 2 mM *n*-dodecyl-β-D-maltopyranoside, and 0.3 mM cholesterol hemisuccinate were concentrated to 2 mg/mL (MWCO 100 kDa) with either 1 mM 2S,4R-4-methylglutamate or 1 mM LY466195 and snap-frozen in liquid nitrogen. Fluorescence-detection size-exclusion chromatographic analysis revealed no change in chromatographic behavior after samples were thawed for structural analysis.

1. Alushin GM, Jane D, Mayer ML (2011) Binding site and ligand flexibility revealed by high resolution crystal structures of GluK1 competitive antagonists. *Neuropharmacology* 60(1):126–134.

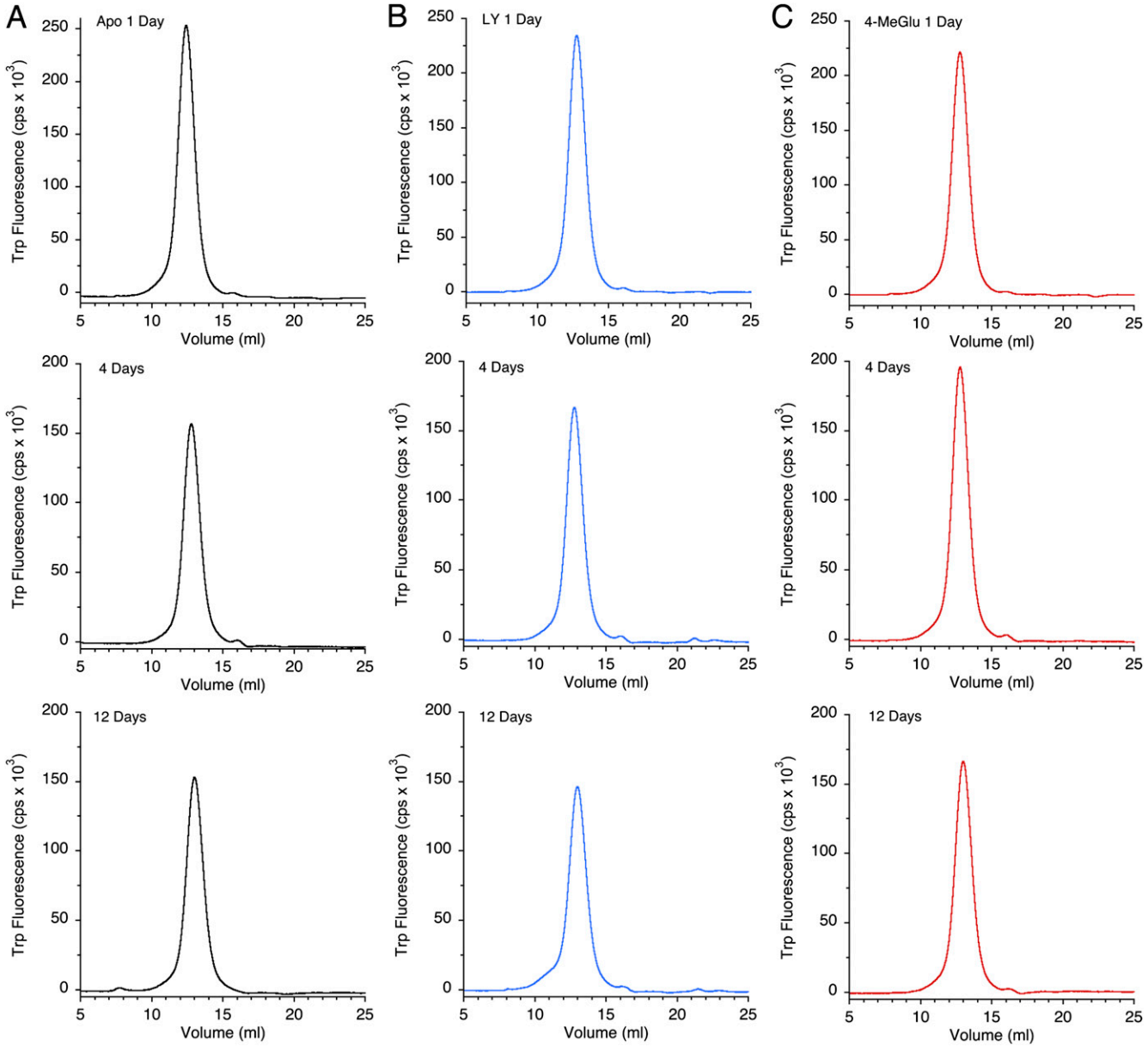

Fig. S1. Analytical gel filtration chromatograms for GluK2 samples stored at 4 °C for 1, 4, and 12 d following purification for (*A*) the apo state and for complexes with 1 mM concentrations of either (*B*) LY466195 or (*C*) 2S,4R-4-methylglutamate.

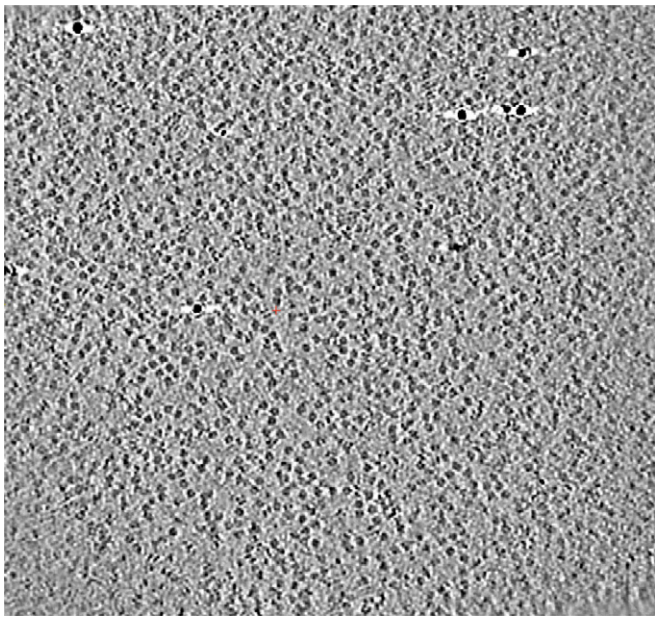

Fig. S2. Representative tomographic slice of vitreous ice-embedded GluK2 receptors obtained by cryoelectron tomography illustrating a typical field of view in electron micrographs. The images shown in Fig. 1 *B* and *C* are from images such as the one shown here.

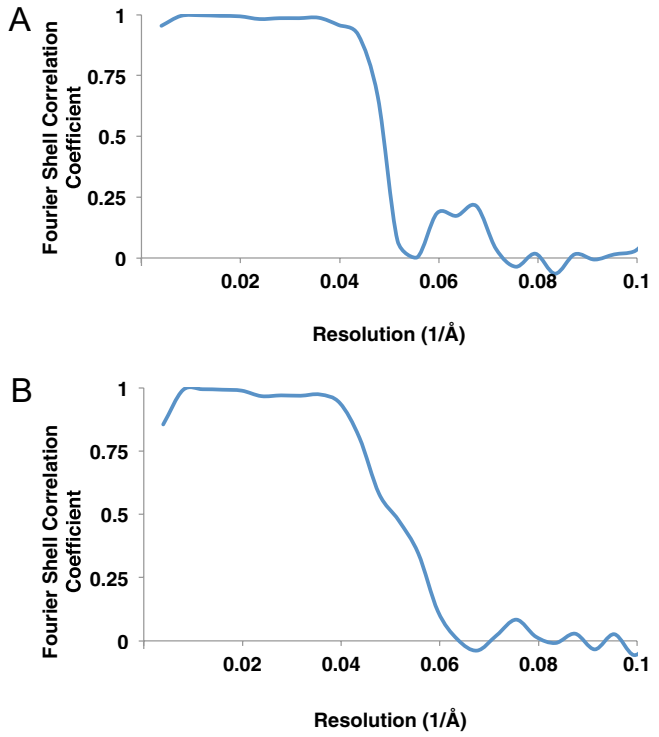

Fig. S3. Plots of the resolution dependence of the Fourier shell coefficient between two random halves of the volumes used to obtain the 3D structures presented for GluK2 in antagonist-bound (*A*) and desensitized (*B*) states. The plots show that the correlation coefficient drops to values of 0.5 at resolutions of ~21 Å, which is therefore used as a nominal estimate of the resolution of the density maps.

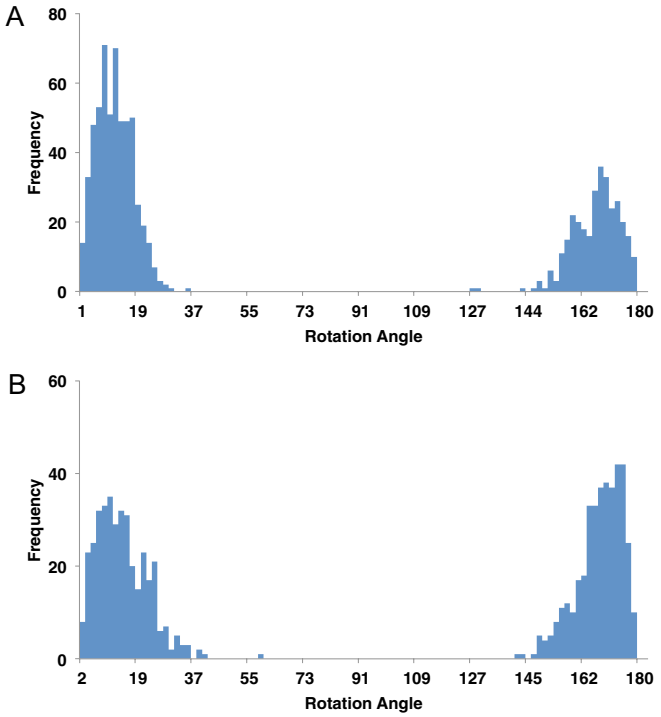

Fig. S4. Histogram of orientations assigned to each molecular volume of GluK2 in antagonist-bound (*A*) and desensitized (*B*) states. The horizontal axis represents the magnitude of the angular deviation of each molecule from the long axis of the averaged map (i.e., the direction of the twofold axis). The plot confirms that the GluK2 molecules display preferential orientation, with molecules roughly aligned with the twofold axis and an approximately even distribution between "up" (angles between 0° and 30°) and "down" (angles between 150° and 180°) orientations. Interestingly, the most populated orientation is slightly tilted (~20°) from the normal to the plane of the carbon film. The presence of preferred orientation is also evident from inspection of the tomographic slices in Fig. 1 and Fig. S2.

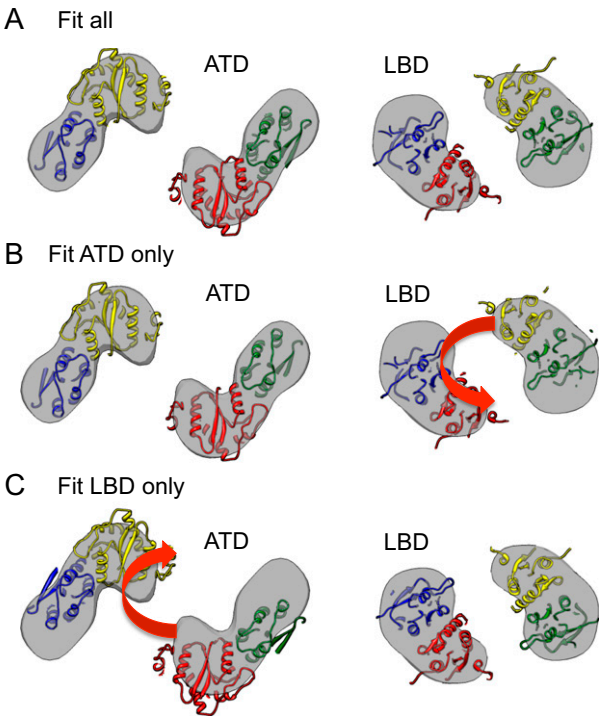

Fig. S5. Comparison of molecular structure of GluK2 and $GluA2_{cryst}$ in the resting state. (*A*) Slices through resting-state density maps for GluK2 fitted with $GluA2_{cryst}$ coordinates using the entire receptor. The slices show fits at the approximate center of the ATD (*Left*) and LBD (*Right*) regions. (*B*) Fits of ATD and LBD domains when the fitting is done using only the ATD portion of $GluA2_{cryst}$ coordinates. (*C*) Fits of ATD and LBD domains when the fitting is done using only the LBD portion of GluA2 $GluA2_{cryst}$ coordinates. The fitting experiments show that an anticlockwise twist of the LBD relative to the ATD (when the receptor is viewed from the top toward the membrane) results in a better fit than when the fitting is done with intact 3KG2 coordinates.

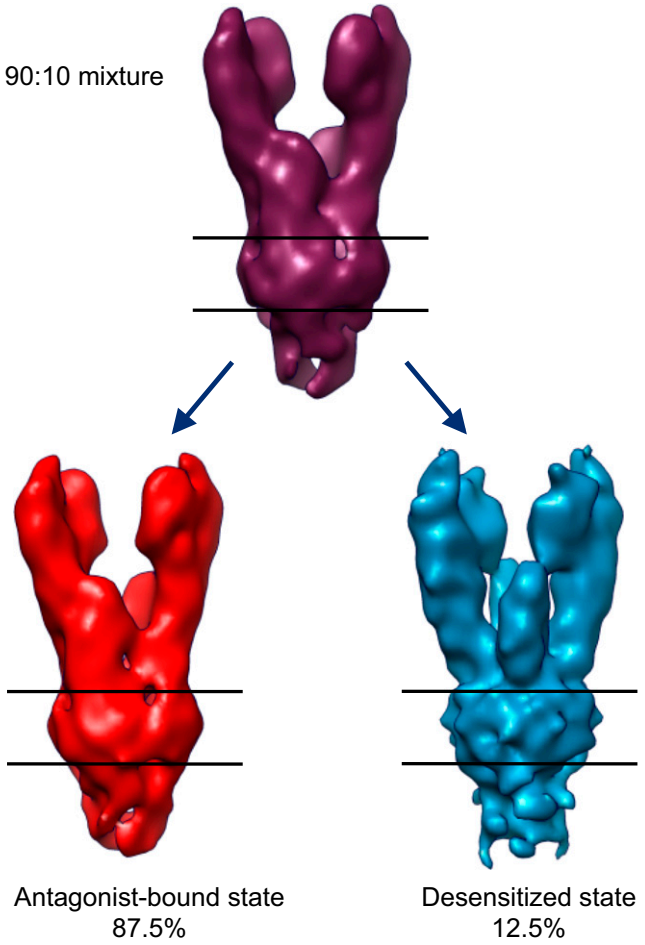

Fig. S6. Demonstration that a computationally labeled mixture of receptors in resting and desensitized states can be separated successfully when the minority conformation is present at a tenth of the concentration of the dominant conformation. A computational mixture of 2,000 receptors was prepared by mixing 1,800 subvolumes derived from samples in the resting state and 200 subvolumes derived from samples in the desensitized state where the large conformational change is observed. The averaged structure derived from the mixture (magenta) is essentially indistinguishable from that of the resting state. However, after the mixture was then subjected to iterative reference-free classification, the minority population (blue) is clearly separated from the majority population (red). The final numbers derived for the relative amounts are about 87.5% and 12.5%, providing a measure of the fidelity of the all of the steps involved in the structural analysis.

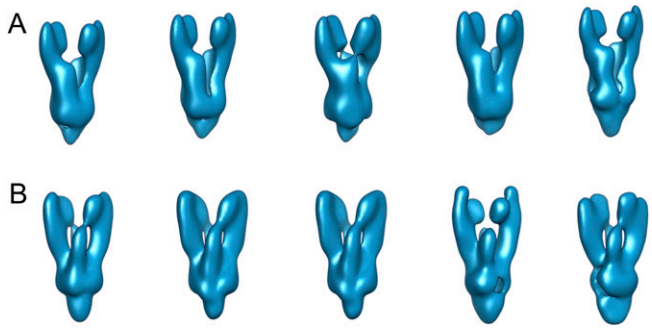

Fig. S7. Results from classification of GluK2 molecular volumes following collaborative alignment to obtain averaged 3D structures. The classification tree is essentially "flat," and the averages of subsets of the dataset from GluK2 in antagonist-bound (*A*) and desensitized (*B*) states are all similar to each other, and to the corresponding global averaged structures. The absence of measurable conformational heterogeneity is in contrast to the results from classification where we explicitly mixed molecular volumes with distinct conformation (Fig. S6).

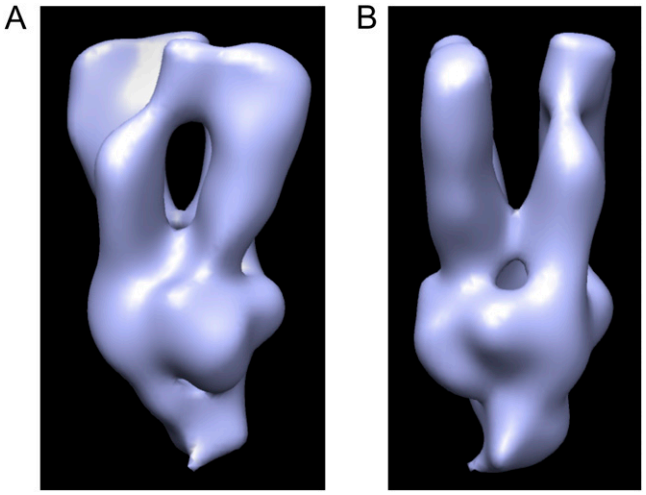

Fig. S8. Subvolume averages obtained from 105 subvolumes of GluK2 in the desensitized state processed without any symmetry imposed. (*A* and *B*) Two front views, rotated by ~90° around the long axis. Despite the small number of volumes and the lower resolution, the separation of the ligand-binding domain into four lobes is clearly delineated.

Movie S1. Superposition of density maps for GluK2 in resting (blue) and desensitized (yellow) states derived by cryoelectron tomography and subvolume averaging at ~21 Å resolution.

Movie S1

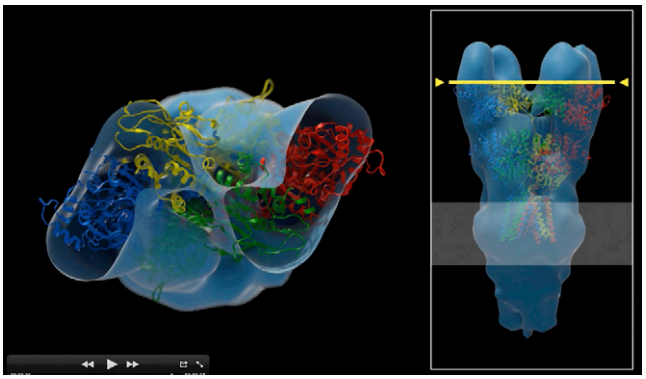

Movie S2. Fit of GluA2 coordinates determined by X-ray crystallography into the GluK2 resting-state density map determined by cryoelectron tomography and subvolume averaging.

Movie S2